www.czasopisma.pan.pl PAN POLSKA AKADEMIA NAUK www.journals.pan.pl

Arch. Metall. Mater. **64** (2019), 2, 765-771

DOI: 10.24425/amm.2019.127611

J. ZYCH*, J. PIEKŁO*, M. MAJ*, A. GARBACZ-KLEMPKA*#, M. PIĘKOŚ*

INFLUENCE OF STRUCTURAL DISCONTINUITIES ON FATIGUE LIFE OF 4XXX0-SERIES ALUMINUM ALLOYS

Fatigue investigations of two 4XXX0-series aluminum alloys (acc. PN-EN 1706) within a range of fewer than 10^4 cycles at a coefficient of cycle asymmetry of $R = -1$ were performed in the current paper. The so-called modified low-cycle test, which provided additional information concerning the fatigue life and strength of the tested alloys, was also performed. The obtained results were presented in the form of diagrams: stress amplitude σ_a – number of cycles before damage N. On the basis of the microscopic images of sample fractures, the influence of the observed casting defects on the decrease of cycle numbers at a given level of stress amplitude were analyzed. Based on the images and dimensions of the observed defects, stress intensity factor K_I was analytically determined for each. Their numerical models were also made, and stress intensity factor K_I was calculated by the finite element method (FEM).

Keywords: aluminum alloys, casting defects, material fatigue, fracture mechanics, numerical calculations of FEM

1. Introduction

The design of lighter and lighter structure elements requires wider knowledge concerning the applied material and its behavior under the influence of various kinds of loads. This also concerns aluminum alloys, which have been successfully applied in the automotive and aircraft industry on account of their very advantageous strength-to-mass ratio. Problems regarding the improvement of the quality of aluminum-based alloys have been the subjects of numerous investigations [1-5]. Castings made of aluminum alloys usually contain various structural discontinuities, which have an essential influence on the strength and fatigue life of these alloys. Investigations related to the influence of precipitates and structural defects on alloy durability have been presented in several papers, of which the papers of Y. Murakami [6,7] should be quoted. Structural discontinuities can constitute spaces unfilled with metal or non-metallic inclusions, which decrease the mechanical properties of castings [8]. Liquid aluminum has a tendency to adsorb hydrogen and oxidize, which are reasons for the unavoidable presence of gaseous porosity and oxide inclusions in aluminum castings. When the casting is not properly supplied, its fatigue life can be additionally decreased by shrinkage porosity. The gaseous porosity is usually of a round shape, while the shrinkage porosity forms irregular three-dimensional voids [9]. Both types of porosity can occur along with aluminum oxide films. Structural discontinuities and various voids caused by porosities can have different sizes; thus, microporosity can be singled out when the diameter or the largest size of a void does not exceed 100 μm, and porosity can be identified when the void size is larger than 100 μm [10]. Porosity and microporosity greatly shorten fatigue life and decrease alloy strength, while microporosity alone only decreases fatigue life in large number of cycles [11,12]. The microporosity influence should be considered in connection with the features of the alloy microstructure, since the location of the microcrack-initiation sites depends on the mutual ratio of the dimensions and distances of the voids and phases in the microstructure [6]. During investigations of the fatigue life of aluminum alloys, a large scatter of results related to the porosity is often observed. During our investigations, the fatigue fractures of the samples were subjected to a microscopic analysis to discover the eventual material discontinuity. In the case of revealing the macroporosity in which the diagonal length measured in the sample fracture plane (perpendicular to the force direction) was greater than 0.9 mm, methods of cracking mechanics were applied, and stress intensity factor K_I was determined.

2. Applied investigation methodology

The analysis of the fatigue life of aluminum alloys and the influence of the detected macroporosities on decreasing the strength were performed on the basis of fatigue investigations within a small number of cycles and by means of the so-called modified low-cycle fatigue test (carried out by the MTS 810 strength machine) as well as by applying methods of cracking mechanics. The fractures were analyzed on the basis of pictures obtained by means of a stereoscopic microscope and electron

* AGH UNIVERSITY OF SCIENCE AND TECHNOLOGY, FACULTY OF FOUNDRY ENGINEERING, 23 REYMONTA STR., 30-059 KRAKOW, POLAND

Corresponding author: agarbacz@agh.edu.pl

scanning microscope. The method of the modified low cycle fatigue test and the calculating method of stress intensity factor K_I, are briefly discussed below.

2.1. Modified low-cycle fatigue test

In order to determine several mechanical properties, the modified low-cycle fatigue test (MLCF) was applied. This method description oriented towards problems concerning foundry alloys and their theoretical bases is presented in [13]. An example of this method of application in analyzing the casting of an automotive vehicle suspension (a so-called "rocker" made of an AlZnMgCu alloy) that allowed us to determine Parameters b and c resulting from the Manson-Coffin-Morrow dependence can be found in [14]:

$$\frac{\Delta\varepsilon_{sp}}{2}+\frac{\Delta\varepsilon_{pl}}{2}=\frac{\sigma_f'}{E}\left(2N_f\right)^b+\varepsilon_f'\left(2N_f\right)^c \tag{1}$$

$\Delta\varepsilon_{ap}$ – plastic strain amplitude,
$\Delta\varepsilon_{ae}$ – elastic strain amplitude,
$2N_f$ – number of cycles,
n – exponent of the cyclic strengthening,
ε_f' – coefficient of the cyclic plastic strain,
σ_f' – coefficient of the fatigue life,
E – elasticity modulus.

According to the MLCF procedure, tests were performed on samples with a diameter of 8.0 mm applying a positive response-pulsating cycle of $R = 0$ with a growing stress amplitude up to the sample fracture.

2.2. Crack mechanics as related to macroporosity type

Notches and holes cause a concentration of stresses in their direct vicinity. These stresses are much higher than nominal stress σ_{nom} in places that are a certain distance from the notches and holes. Fatigue cracks are most often initiated in zones of stress concentrations.

However, the characteristic of the stress field in the crack vertex is quite different than in the case of a hole or notch. The explanation of the stress concentration near discontinuities of various shapes is crucial for the formulation of quantitative assessments of the influence of small defects such as cracks and non-metallic inclusions on the fatigue strength of casting alloys. When a crack propagates from the stress concentration zone, the problem should be considered from the crack mechanics point of view rather than as the problem of stress concentrations by notches or holes. Therefore, stress intensity factor K_I dependent on the crack geometry (determined by parameter "Y" and limit conditions) constitutes the basic value on which it is possible to estimate the crack resistance changes.

$$K_I=\sigma_{nom}\sqrt{\pi a}\cdot Y \tag{2}$$

When it is assumed that the crack surface is placed in the middle of a disk plate of infinitely large dimensions perpendicular towards the direction of stress operations σ_{nom}, Equation (2) will be simplified to the following form:

$$K_I=\sigma_{nom}\sqrt{\pi a} \tag{3}$$

The shape of the small defects (including the casting defects) differs from the classic model of a crack surface considered by crack mechanics. On account of this, the so-called surface parameter "A" was introduced. When the discontinuity is of a regular shape, the geometrical parameter is equal to the surface of the defect [15].

$$K_I=\alpha\cdot\sigma_{nom}\sqrt{\pi\sqrt{A}} \tag{4}$$

When the defect is inside the casting wall, the coefficient is $\alpha = 0.5$; when it is on the surface, $\alpha = 0.6$. In the case of an irregular perimeter of a defect, the geometrical parameter is determined by the surface formed by the perimeter of the original contour of discontinuity. When the defect is situated perpendicularly to the operation direction of nominal stress σ_{nom}, surface parameter "A" is equal to the defect surface.

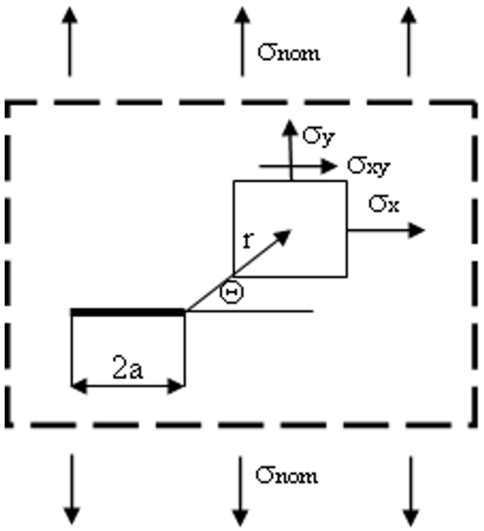

Fig. 1. Components of stress in vicinity of crack vertex of length 2a

2.3. Description of investigation procedure

Fatigue tests were performed by using round samples of a diameter of $\phi = 8$ mm and a measuring base of $l = 20$ mm. The samples were cut out from sand-cast plates with a thickness of 10 mm and subjected to heat treatment T6 while maintaining the following parameters: hyperquenching at $T_p = 540$°C for 4h; cooling in water at a temperature of $T_{co} = 55$-60°C; and aging at a temperature of $T_{ag} = 180$°C for 12h. During the low-cycle LCF fatigue test, four samples with one stress amplitude level were tested for the No. 1 and No. 2 alloys, and the average values were determined during the MLCF test based on three measurements. For both tested alloys of the chemical composition given in Table 1, the same heat treatment was applied. The samples were tested by means of the MTS 810 hydraulic testing machine. In the case of

the low-cyclic fatigue test, the fatigue course was controlled by the sinusoidal change of the force value in the cycles of asymmetry coefficient $R = -1$. The investigations were carried out at a frequency of load changes of 0.5 Hz within a range of 20 to 10^4 numbers of cycles. The surfaces of the sample fractures were tested by means of the stereoscopic microscope and (in selected cases) by means of the scanning microscope. In the so-called MLCF (modified low cycle fatigue test), the sinusoidal cycle was controlled by changes of force, whose value was increased by 0.5 kN every twenty cycles up until the sample fractured.

TABLE 1

Percentage fractions of alloy components in tested Alloys No. 1 and No. 2

Alloy	Contents of elements (wt.%)							
	Si	Fe	Cu	Mg	V	Ti	B	Al
No. 1	7.32	0.069	0.98	0.579	—	0.179	—	90.8
No. 2	6.81	0.075	—	0.47	0.01	0.244	0.012	92.4

3. Results of investigations

Several parameters characterizing the mechanical properties of the alloys (Table 2) were determined on the basis of investigations performed by means of the modified low-cyclic fatigue tests. Some of them can be compared with the results obtained during the static tensile tests. The strength and fatigue properties of the alloys determined during the modified low-cyclic fatigue tests are listed below:

- UTS – ultimate tensile strength,
- A – elongation,
- E_0 – initial elasticity modulus,
- E_{10}, E_{80}, E_{180} – elasticity module at loads of 10, 80, and 180 MPa, respectively,
- $R_{0.02}$ – apparent proportionality limit for 0.02% elongation,
- $R_{0.05}$ – apparent elastic limit for 0.05% elongation,
- $R_{0.1}$ – apparent elastic limit for 0.1% elongation,
- $R_{p0.2}$ – apparent plasticity limit for 0.2% elongation,
- Z – fatigue strength limit,
- ε_{max} – highest permissible deformation in fatigue test.

On the basis of the fatigue tests, the Manson-Coffin-Morrow coefficients and the remaining coefficients were determined for Alloy No. 1:

$$\frac{\Delta\varepsilon_{sp}}{2}+\frac{\Delta\varepsilon_{pl}}{2}=0.006\left(2N_f\right)^{-0.066}+0.057\left(2N_f\right)^{-0.897} \quad (4)$$

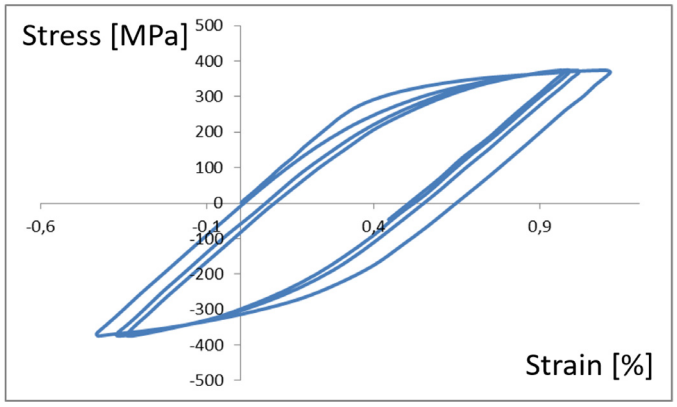

Fig. 2. First three fatigue cycles during investigating Alloy No. 2: values for stabilized hysteresis loop are σ_a = 375.1 MPa (10.6 kN), ε_{ap} = 0.0675%, ε_{ae} = 0.4%, ε_{ac} = 0.4675%, and $2N_f$ = 212 cycles

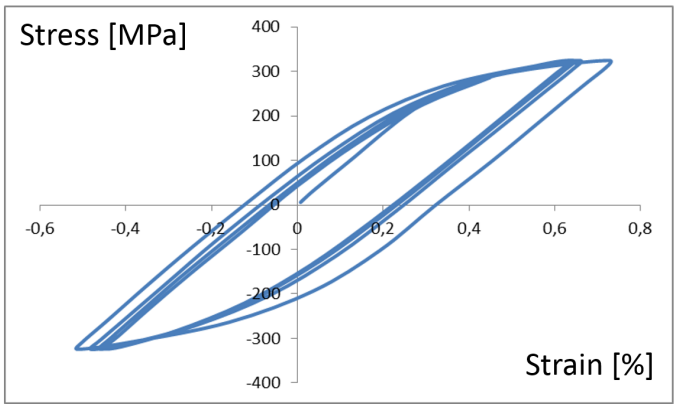

Fig. 3. First three fatigue cycles during investigating Alloy No. 2: values for stabilized hysteresis loop are σ = 325.5 MPa (9.2 kN), ε_{ap} = 0.104%, ε_{ae} = 0.423%, ε_{ac} = 0.527%, and $2N_f$ = 27 cycles

and for Alloy No. 2:

$$\frac{\Delta\varepsilon_{sp}}{2}+\frac{\Delta\varepsilon_{pl}}{2}=0.004\left(2N_f\right)^{-0.072}+0.008\left(2N_f\right)^{-0.712} \quad (5)$$

Examples of the hysteresis loops obtained after the first three cycles for both alloys are shown in Fig. 2 and 3. Fatigue life diagrams prepared of the bases of Equations (4) and (5) are presented in Fig. 4 and 5. The cyclic deformations of Alloy No. 1 provides Equation (6), while for Alloy No. 2 – Equation (7). The correlation coefficients are equal to R = 0.93 for Alloy No. 1 and R = 0.98 for Alloy No. 2.

$$\sigma_a = 433(\varepsilon_{ap})^{0.0575} \quad (6)$$

TABLE 2

Results of static tensile tests (marked 'Tt') and modified low-cycle fatigue tests (marked 'MLCF' for Alloys No. 1 and No. 2)

Alloy	UTS	A	E_{180}	$R_{0,02}$	$R_{0,05}$	$R_{0,1}$	$R_{p0,2}$	Z	ε_{max}
	[MPa]	[%]	[MPa]	[MPa]	[MPa]	[MPa]	[MPa]	[MPa]	[%]
No. 1 Tt	395	3.54	79.000	—	—	—	326	—	—
No. 1 MLCF	389	—	83.600	221	246	301	325	126	0.02
No. 2 Tt	356	1.50	81.000	—	—	—	320	—	—
No. 2 MLCF	326	—	84.900	189	237	262	288	110	0.001

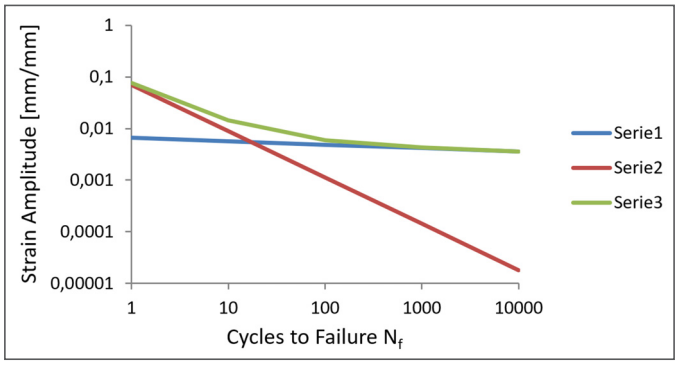

Fig. 4. Diagram of fatigue life of Alloy No. 1: Series 1 – elastic strain ε_{ae}; Series 2 – plastic strain ε_{ap}; Series 3 – total strain ε_{ac}

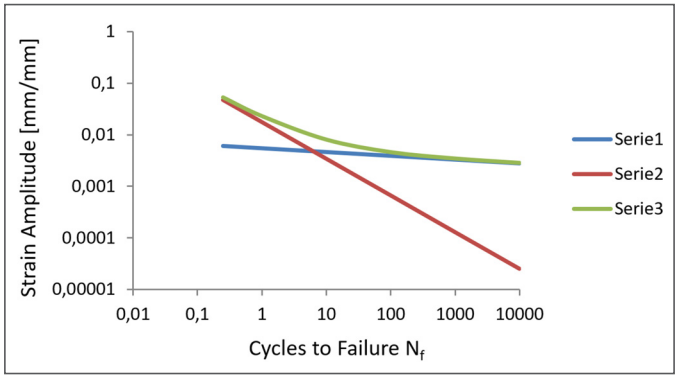

Fig. 5. Diagram of fatigue life of Alloy No. 2: Series 1 – elastic strain ε_{ae}; Series 2 – plastic strain ε_{ap}; Series 3 – total strain ε_{ac}

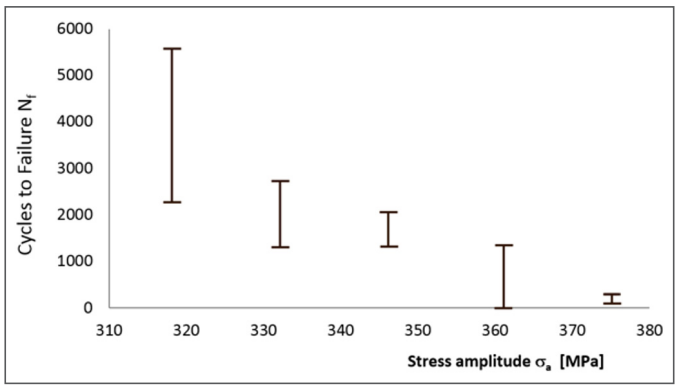

Fig. 6. Dependence of stress amplitude σ_a and number of cycles leading to damage determined on Alloy No. 1

$$\sigma_a = 380.8(\varepsilon_{ap})^{0.059} \tag{7}$$

During the performance of the fatigue tests within a range of a low number of cycles, significant differences between the number of cycles leading to the sample fractures tested at the same levels of stress were found. To depict this fact, diagrams of the difference between two minimum and maximum numbers of cycles $2N_f$ (Fig. 6) and stress amplitude σ_a (Fig. 7) were prepared. In the samples that were damaged after the lower number of cycles at the same level of stress amplitude σ_a, the occurrence of casting defects was found in several cases. The presence of the defects was confirmed by microscopic tests.

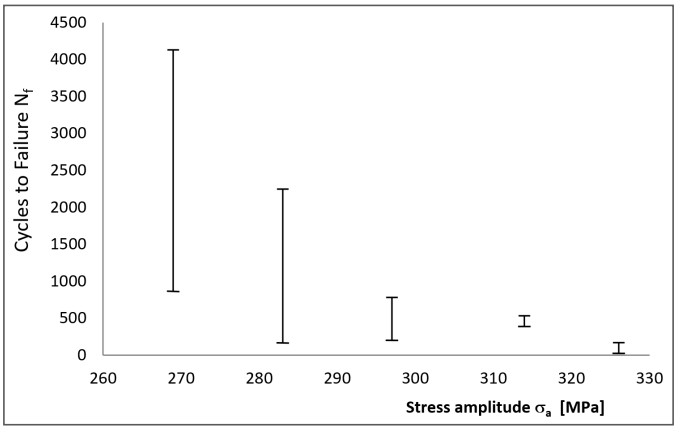

Fig. 7. Dependence of stress amplitude σ_a and number of cycles leading to damage determined on Alloy No. 2

3.1. Morphology of fractures

The fractures of the samples after the fatigue tests were subjected to analysis in order to confirm the presence of eventual non-metallic inclusions, porosities, or oxide films as well as determine their influence on decreasing the fatigue life as compared to the remaining samples in which such a structure discontinuity was not found. Calculating analyses were performed in the cases when the revealed defects were large enough to allow us to rule out the microstructure influence and to state explicitly that they are the initiators of the cracks. A typical fatigue fracture on which surface defects were not found is shown in Fig. 8. Three zones can be singled out on this fracture: initiation "A"; propagation "B"; and the very rapid increase of the fatigue in crack "C". Stress amplitude σ_a was equal to 318 MPa, and the number of cycles until the moment of fracture was $2N_f = 5600$. On account of the relatively low alloy plasticity, the zone with a very rapid increase of fatigue crack "C" is very large

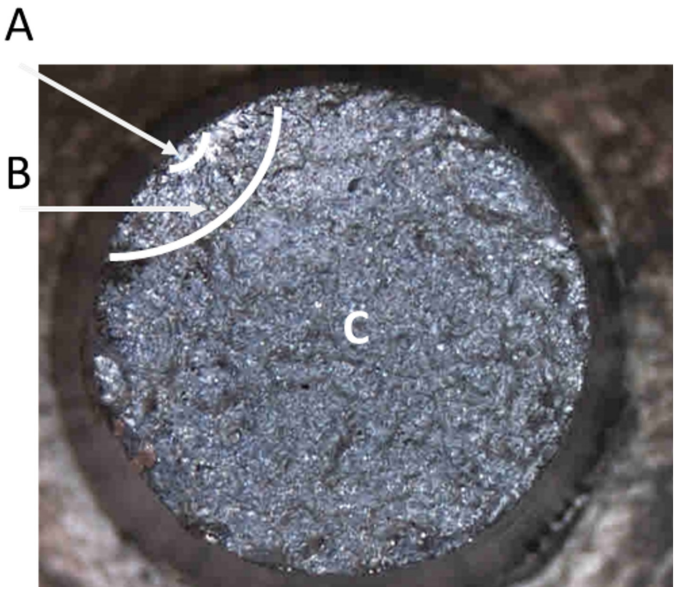

Fig. 8. Fatigue fracture with single place of crack initiation – Alloy No. 1: stress amplitude – $\sigma_a = 318$ MPa; number of cycles to moment of fracture – $2N_f = 5600$

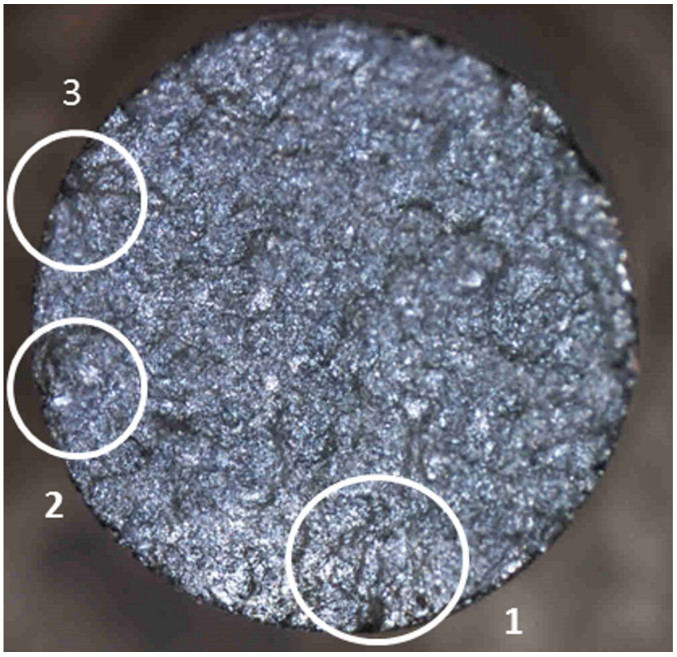

Fig. 9. Fatigue fracture with three marked crack initiation zones – Alloy No. 1: stress amplitude – σ_a = 361 MPa; number of cycles to moment of fracture – $2N_f$ = 1386

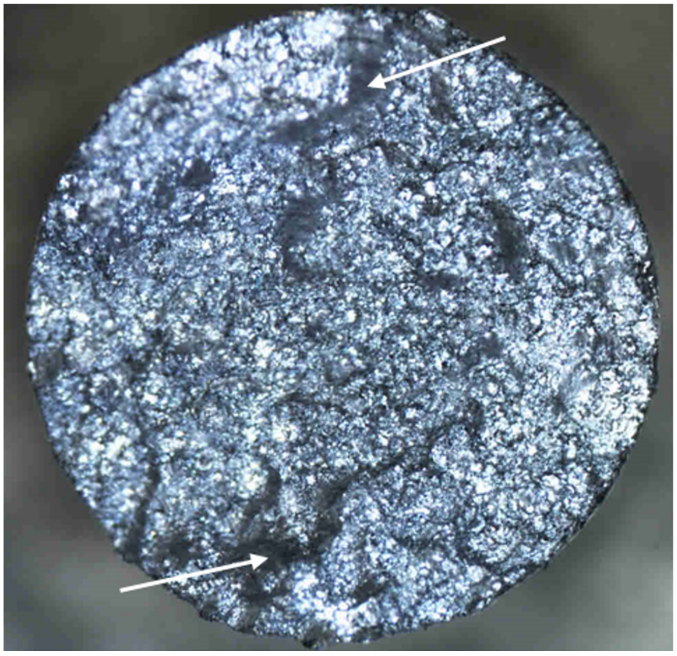

Fig. 10. Two cracks initiated from porosity zone (market by arrows) – Alloy No. 1: stress amplitude – σ_a = 292.7 MPa; number of cycles to moment of fracture – $2N_f$ = 470

In some cases, it was possible to observe several simultaneously developing crack initiation places when the stress amplitude was greater than 318 MPa. The example of such fracturing is presented in Fig. 9. In cast alloys (including aluminum alloys), several defects occur (which could initiate cracks); however, their propagation depends on the stress value. When this value is too low, the increase in cracking stops. Shrinkage, gaseous porosity, and oxide films can also be sites of crack initiation. An example of a crack initiated from the porosity zone can be seen in Fig. 10.

The photographs of the fractures taken by means of the scanning microscope indicate the places and shapes of the porosities located in various places of the sample fracture surfaces (Fig. 11).

3.2. Numerical model of cracking initiation from defect zone

When defects in the form of a porosity or non-metallic precipitates from which the developing cracks were initiated occurred on the sample fracture, a numerical model of the defect was performed and FEM calculations were done in order to determine stress intensity factor K_I in selected places of the outline of the defect surface. The collected results of the performed calculations are presented in Table 3. An example of a model of one defect found in the fracture is shown in Fig. 12. In addition, the value of factor K_I for geometrical models of the defects was analytically determined on the bases of Equations (1), (2), and (3).

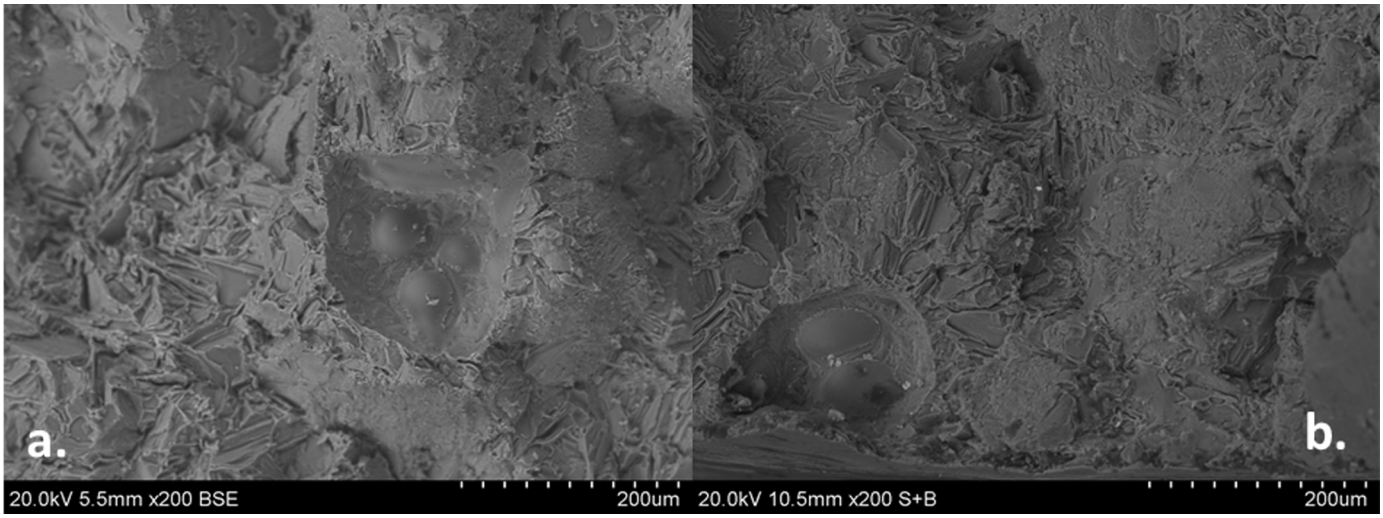

Fig. 11. Fatigue fracture of Alloy No. 2: (a) porosity near sample axis and (b) porosity at sample edge can be seen

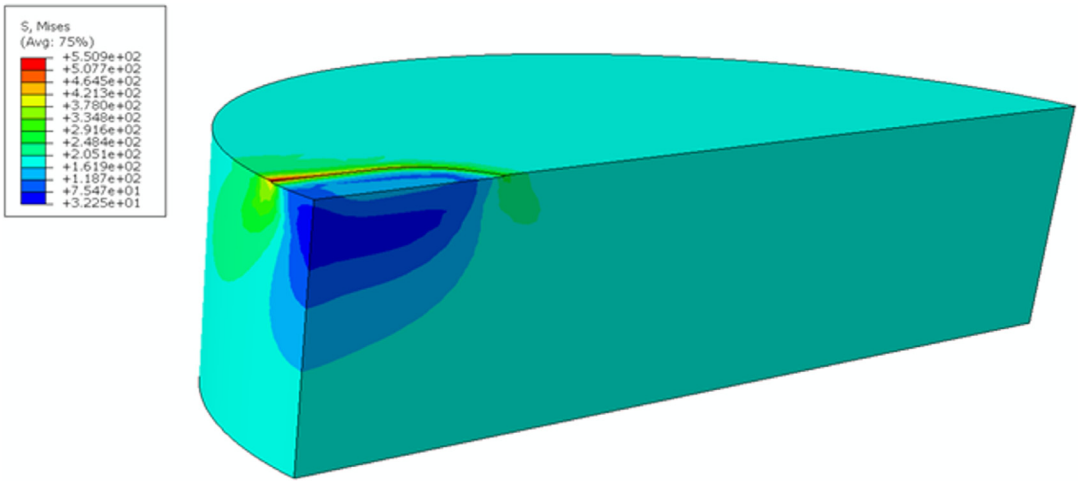

Fig. 12. Geometrical model and picture of local increase of reduced stresses according to Huber-Mises hypothesis in vicinity of defect

TABLE 3

Values of stress intensity factor K_I determined numerically (FEM) on basis of Equation (1) K_I (crc) and Equation (3) K_I (sue) together with corresponding number of cycles before moment of fracture $2N_f$ and stress amplitude σ_a determined using low-cycle fatigue tests marked (LCF for Alloys No. 1 and No. 2)

Alloy	σ_a [MPa]	$2N_f$	K_I (FEM)	K_I (crc)	K_I (sue)
No. 1 LCF	332.6	1323	12.1	18.8	11.1
No. 1 LCF	346.7	1340	11.8	18.3	10.9
No. 1 LCF	360.9	790	13.3	19.1	12.1
No. 2 LCF	268.9	865	8.2	11.3	7.7
No. 2 LCF	283.0	165	11.2	12.9	10.7

The outline of the defect (Fig. 13) was divided into three parts by two straight lines joined by an arc. On each curve, the coordinates of the points in which the stress intensity factor obtains the maximal value were numerically determined. These points coincide quite well with the crack initiation place seen in the sample fracture. Two directions of the cracks, the propagation of which led to the sample fracture, are shown by the arrows that start in the rectilinear part of the outline where the value of stress intensity factor K_I equals 13.3 MPa·m$^{0.5}$.

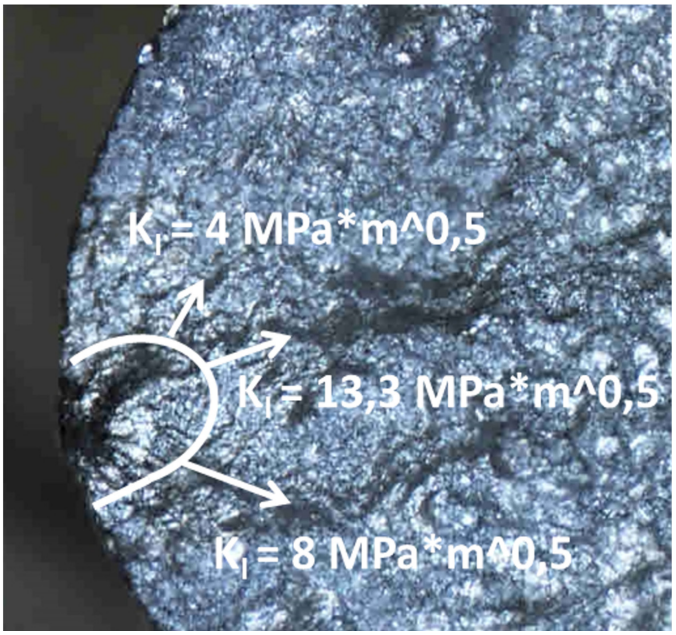

Fig. 13. Stress intensity factor K_I determined by means of FEM at three points of outline of defect surface

4. Conclusions

The performed investigations indicated the significant influence of casting defects on the fatigue life properties of the tested 4XXO-series alloys. The obtained results show large differences in the number of cycles before damage occurred between samples loaded by the same stress amplitude. These differences were dependent on the size and location of the defect. In the majority of cases, the crack initiates from the defect edge near the external cylindrical sample surface. The number of zones of fatigue crack initiation identified on the fracture surface also influenced the number of cycles before the moment of sample fracturing. In the case when crack initiation was caused by the defect, its geometrical model was determined, and calculations aimed at determining stress intensity factor K_I were performed. In the case of samples with identified casting defects, it was found (Table 3) that, regardless of the stress amplitude, the number of fatigue cycles before the moment of sample fracture is smaller the higher stress intensity factor K_I is. Such a relationship occurred in all of the analyzed cases (independent of the assumed calculating model) in spite of the differences in the determined stress intensity factor K_I. Assuming the defect model in the form of a linear gap (Equation 3), causes that the stress intensity factor has – in certain cases – a much higher value than the one calculated by means of the FEM (the true shape of the defect) or Equation (4). The difference is caused by the discrepancy between the real shape of the defect and the crack model.

Copper increases the strength, hardness, workability, and thermal conductivity of aluminum alloys. The increase in the content of this element in the alloy causes an increase in volume

and the growth of zones between dendrites rich in copper. Heat treatment gives the best results with the addition of 4-6% Cu. A small addition of 0.5% of copper has a positive effect on the abrasion resistance of the A356 alloy [16]. According to the authors of the work [17] the greatest increase in the yield point $R_{p0.2}$ occurs when the Cu content is between 1-1.6%, and that with the Cu increase the formation temperature of the Al_2Cu phase decreases. The addition of copper mainly affects the course of the crystallization process [17]. Changes in the strength and mechanical properties of the alloy are the result of the effect of the addition of copper on the crystallization process

REFERENCES

[1] E.R. Wang, X.D. Hui Shushen Wang, G.L. Chen, Materials Science and Engineering **A 527** (29), 7878-7884 (2010). DOI: 10.1016/j.msea.2010.08.058

[2] N.D. Alexopoulos, Sp.G. Pantelakis, Journal of Materials Engineering and Performance **12** (2), 196-205 (2003). DOI: 10.1361/105994903770343358

[3] E. Czekaj, J. Nykiel, Z. Kwak, A. Garbacz-Klempka, M. Nykiel, Archives of Foundry Engineering **18** (2), 72-78 (2016). DOI: 10.24425/122505

[4] E. Czekaj, J. Zych, Z. Kwak, A. Garbacz-Klempka, Archives of Foundry Engineering **16** (3), 25-28, (2016). DOI: 10.1515/afe-2016-0043

[5] S. Rzadkosz J. Zych, M. Piękoś, J. Kozana, A. Garbacz-Klempka, J. Kolczyk, Ł. Jamrozowicz, Metalurgija **54** (1), 35-38 (2015).

[6] Y. Murakami, Metal Fatigue: Effects of Small Defects and Nonmetallic Inclusions, Elsevier Science (2002).

[7] H. Kobayashi, H. Ikeda, Y. Murakami, Transactions of the Japan Society of Mechanical Engineers Ser. A **62** (594), 347-355 (1996).

[8] H. Mayer, U. Fuchs, S. Tschegg, B. Zettl, Hj. Lipowsky, A. Stich, M. Papakyriacou, Materials Science & Materials Engineering **33** (3), 117-127 (2002). in German

[9] X.B. Cao, J. Zhao, J.H. Fan, M.H. Zhang, G.J. Shao, Q. Hua, International Journal of Cast Metals Research **27** (6), 362-368 (2014).

[10] K. Gal, N. Yang, M. Horstemayer, D.L. McDowell, J. Fan, Metallurgical and Materials Transactions **30A** (December), 3079-3088 (1999).

[11] Q.G. Wang, D. Apelian, D.A. Lados, Journal of Light Metals **1**, 73-84 (2001).

[12] Q.G. Wang, D. Apelian, D.A. Lados, Journal of Light Metals **1**, 85-97 (2001).

[13] M. Maj, K. Pietrzak, J. Piekło, Archives of Metallurgy and Materials **58** (3), 877-881 (2013).

[14] S. Pysz, E. Czekaj, R. Żuczek, M. Maj, J. Piekło, Archives of Foundry Engineering **16** (1), 55-60 (2016).

[15] Y. Murakami, Engineering Fracture Mechanics **22**, 101-114 (1985).

[16] M.S. Prabhudev, V. Auradi, K. Venkateswarlu, N.H. Siddalingswamy, S.A. Kori, Procedia Engineering **97**, 1361-1367 (2014). DOI: 10.1016/j.proeng.2014.12.417

[17] P. Suwanpinij, U. Kitkamthorn, I. Diewwanit, T. Umeda, Mater. Trans. **44** (5), 845-852 (2003).